Dynamic causal modelling shows a prominent role of local inhibition in alpha power modulation in higher visual cortex

Frederik Van de Steen[1,2,3*], Dimitris Pinotsis[4,5], Wouter Devos[1], Nigel Colenbier[1,6,7], Iege Bassez[1], Karl Friston[3] and Daniele Marinazzo[1]

[1] Department of Data Analysis, Ghent University, Ghent, Belgium

[2] Vrije Universiteit Brussel, Brussel, Belgium, AIMS laboratory.

[3] The Wellcome Trust Centre for Neuroimaging, University College London, London, United Kingdom

[4] Centre for Mathematical Neuroscience and Psychology and Department of Psychology, City - University of London, London, EC1V 0HB, United Kingdom

[5] The Picower Institute for Learning & Memory and Department of Brain and Cognitive Sciences, Massachusetts Institute of Technology, Cambridge, MA, 02139, USA

[6] Research Center for Motor Control and Neuroplasticity, KU Leuven, 3001 Leuven, Belgium

[7] IRCCS San Camillo Hospital, Venice, Italy

[*] Corresponding author: Frederik.van.de.steen@vub.be

Abstract

During resting-state EEG recordings, alpha activity is more prominent over the posterior cortex in eyes-closed (EC) conditions compared to eyes-open (EO). In this study, we characterized the difference in spectra between EO and EC conditions using dynamic causal modelling. Specifically, we investigated the role of intrinsic and extrinsic connectivity—within the visual cortex—in generating EC-EO alpha power differences over posterior electrodes. The primary visual cortex (V1) and the bilateral middle temporal visual areas (V5) were equipped with bidirectional extrinsic connections using a canonical microcircuit. The states of four intrinsically coupled subpopulations—within each occipital source—were also modelled. Using Bayesian model selection, we tested whether modulations of the intrinsic connections in V1, V5 or extrinsic connections (or a combination thereof) provided the best evidence for the data. In addition, using parametric empirical Bayes (PEB), we estimated group averages under the winning model. Bayesian model selection showed that the winning model contained both extrinsic connectivity modulations, as well as intrinsic connectivity modulations in all sources. The PEB analysis revealed increased extrinsic connectivity during EC. Overall, we found a reduction in the inhibitory intrinsic connections during EC. The results suggest that the intrinsic modulations in V5 played the most important role in producing EC-EO alpha differences, suggesting an intrinsic disinhibition in higher order visual cortex, during EC resting state.

Keywords: Dynamic causal modelling; Visual cortex, alpha band, Resting-State EEG

Author summary

One of the strongest signals that can be measured using EEG are so called alpha rhythms. These are neural oscillations that fall within the 8-12Hz frequency range. Alpha rhythms are most prominent when the eyes are closed and are seen at the electrodes placed at the back of the head. In this study, we studied the mechanism of alpha rhythms changes when going from eyes-open to an eyes-closed state. We used a biologically plausible model including different neural populations. We focused on modelling connections within and between different neural sources of the visual cortex and how they are modulated when going from eyes-open to an eyes closed state. We found evidence that inhibitory neurons play an important role in alpha rhythms.

Introduction

Alpha oscillatory EEG activity (i.e., 8-12Hz) during rest—or task-free recordings—is most pronounced during eyes-closed (EC) conditions, over the posterior cortex. During visual stimulation (i.e. eyes-open state, EO) alpha oscillations are suppressed (but see e.g. [1], who showed alpha suppression in a darkened room). Alpha-power modulations have also been observed during working memory [2,3] and visual attention tasks (e.g. [4]). To date, the neural mechanisms underlying alpha activity and modulation (at the scalp level) remain an open question. Several studies have pointed to the role of the thalamus as driving source of cortical alpha [5–7]. More specifically, it is thought that the pulvinar and/or the lateral geniculate nucleus act as primary alpha-pacemaker(s). However, by using electrocorticographic recordings, a recent study showed that alpha waves in the cortex lead alpha activity in the thalamus [8]. Moreover, it has been suggested that cortico-cortical interactions play a prominent role—above and beyond thalamo-cortical dynamics—in the generations of alpha rhythms [9] and that they are associated with conscious perception [10].

There are several difficulties in providing definitive explanations for alpha power differences between EO and EC. First, it is unclear whether we can recover signals from deep brain structures using non-invasive electrophysiological recordings, such as electro-and magnetoencephalography (EEG, MEG; [11,12]). In order to study dynamics in terms of interacting brain regions from EEG and MEG signals, the so-called inverse problem needs to be solved (i.e. source reconstruction, [13,14]). The accuracy of source localization solutions is to date still a matter of debate [11,15,16]. On the other hand, studies using intracranial recordings have high spatiotemporal resolution but due to the invasiveness, these studies are rather rare and usually involve a small number of electrodes and (clinical) sample size. Another disadvantage is that intracranial recordings do not cover the entire brain and are to some extent also susceptible to volume conduction. Finally, many electrophysiological studies that investigated the alpha-band—from a network perspective— have used measures such as

coherence (i.e. modulus of the cross spectrum) and phase information to quantify (functional) connectivity. However, it has been shown that these measures do not provide a unique or complete description of the underlying data generating process that produce spectral data features, such as spectral coherence [17].

One way to address some of these challenges is estimate effective connectivity with dynamic causal modelling (DCM). DCM has been validated, using intracranial and fMRI data, and has been shown to yield efficient source reconstruction [18]. DCM combines a biophysical and an observation model and provides a solution to the inverse problem by assuming biophysical constraints on the hidden source dynamics. Here, we used DCM to explain the underlying neural dynamics of observed spectral differences between EC and EO conditions, with a specific focus on alpha power. We employed DCM for cross spectral densities features, where both amplitude as well as phase information are used for inferring the underlying neural dynamics in terms of directed synaptic connections. We extended the current implementation by augmenting DCM with parameters characterizing state-dependent changes in intrinsic coupling [19,20]. Inspired by a recent study [8], we modelled 3 distinct sources, assumed to be the main sources of EO-EC alpha power difference observed using EEG. These sources were the primary visual cortex (V1 collapsed across hemispheres, due to their proximity) and the bilateral middle temporal visual areas (V5), which were modelled using an established neural mass model based upon canonical microcircuits. Our main goal was to determine whether EO and EC alpha differences can be explained in terms of changes in either extrinsic connections (i.e. between sources) or changes in intrinsic connections (i.e. within a source) or their combination. We used parametric empirical bayes (PEB) to evaluate which specific connections show modulatory (i.e. condition-specific) effects [21,22]. Finally, we examined the contribution of these modulatory parameters— to alpha power—in more detail, using a sensitivity analysis. We envision that the results here serve as a proof of principle that DCM can provide a mechanistic explanation of EO and EC differences in spectral activity. This is

119 important since several studies have shown that the EO to EC alpha power difference is a
120 neural marker of cognitive health [23–25].

121 Materials and Methods

122 Data and pre-processing

123 In this study, 1-minute EEG recordings were taken from 109 subjects, during eyes open and
124 eyes closed resting-state from the EEG Motor Movement/Imagery PhysioNet dataset [26,27].
125 The data was acquired using the BCI2000 system http://www.bci2000.org). The EEG channels
126 were placed on the scalp according to the international 10-10 system [28]. The data was
127 provided in EDF+ format, containing 64 EEG channels, each sampled at 160 Hz. Eyes open
128 resting-state was followed by the eyes-closed condition.

129 The data were pre-processed using EEGLAB running on MATLAB [29]. The 60Hz power line
130 noise was first removed using the Cleanline EEGLAB plugin. Afterwards, the data were high-
131 pass filtered using default settings, with a lower-cut-off of 1Hz. Then, a low-pass filter with high-
132 cut-off of 45 Hz and default settings were applied. Periods of data contaminated with blink
133 artefacts were repaired using independent component analysis. Bad channels were removed,
134 based on visual inspection. Finally, the data were referenced to their average.

135 Power spectral analysis

136 Our first goal was to confirm the well-known effect on posterior alpha power during wakeful
137 state with the eyes closed. Here, we estimated the power spectra from the last 10 seconds of
138 the eyes-open period and the first 10 seconds of the eyes-closed condition. We choose not
139 the use the full 1 minute resting-state recording because we had showed, in a previous study,
140 that connectivity is non-stationary over 1 minute [30]. The power spectrum was obtained using
141 Welch's method (i.e., pwelch.m command in MATLAB): The signal was divided into maximum
142 8 overlapping windows with a 50% overlap between segments. Segments are obtained with a

Hanning window and subsequently decomposed with discrete Fourier transform. This was repeated for every channel, subject and state (i.e., EO and EC). A permutation based paired t-test was conducted by randomly swapping the EO and EC conditions on a subject specific basis. 5000 permutations were performed for the entire frequency x channel data space, during which the permuted T-values were retained. P-values were obtained by calculating the proportion of permuted t-values exceeding the observed t-value (two-tailed). The multiple comparisons problem was addressed using the Benjamini-Hochberg procedure for maintaining the false discovery rate (FDR) at 5% [31].

Canonical microcircuit

In this study, brain sources are modelled with a neural mass model called the 'canonical microcircuitry' [32,33].This model is equipped with four subpopulations per region: superficial and deep pyramidal cells (SP and DP), spiny stellate cells (SS) and inhibitory populations (II). Within each source, the subpopulations are coupled with so-called intrinsic connections, see **Figure 1** for a schematic presentation. The states in each subpopulation are

SS

$$\dot{x_1} = x_2$$
$$U_1 = A_1\sigma(x_3) + u$$
$$\dot{x_2} = \frac{1}{\tau_1}\left(U_1 - G_1 \circ \sigma(x_1) - G_3 \circ \sigma(x_5) - G_2 \circ \sigma(x_3) - 2x_2 - \frac{1}{\tau_1} \circ x_1\right)$$

SP

$$\dot{x_3} = x_4$$
$$U_2 = -A_3\sigma(x_7)$$
$$\dot{x_4} = \frac{1}{\tau_2}\left(U_2 + G_8 \circ \sigma(x_1) - G_7 \circ \sigma(x_3) - 2x_4 - \frac{1}{\tau_2} \circ x_3\right)$$

ii

$$\dot{x_5} = x_6$$
$$U_3 = -A_4\sigma(x_7)$$
$$\dot{x_6} = \frac{1}{\tau_3}\left(U_3 + G_5 \circ \sigma(x_1) + G_6 \circ \sigma(x_7) - G_4 \circ \sigma(x_5) - 2x_6 - \frac{1}{\tau_3} \circ x_5\right)$$

DP

$$\dot{x_7} = x_8$$
$$U_4 = A_2\sigma(x_3)$$
$$\dot{x_8} = \frac{1}{\tau_4}\left(U_4 - G_{10} \circ \sigma(x_7) - G_9 \circ \sigma(x_5) - 2x_8 - \frac{1}{\tau_4} \circ x_7\right)$$

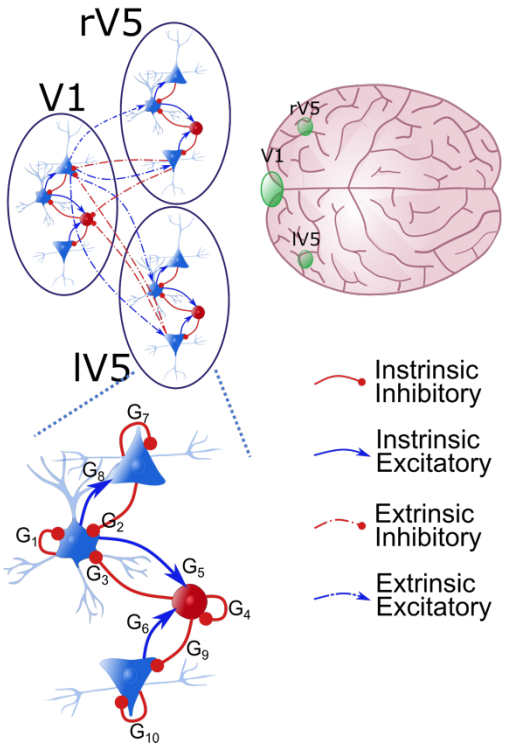

Figure 1. Illustration of the Canonical Microcircuit Model (CMC) model. Each source (V1, rV5 and lV5) comprises 4 neural subpopulations: spiny stellate cells (SS), superficial pyramidal cells (SP), deep pyramidal cells (DP) and inhibitory interneurons (II). Neural populations within a source are coupled with intrinsic connections (full arrows; bottom figure), while coupling between neural populations of different sources are extrinsic connections (dotted arrows). Red and blue arrows denote inhibitory and excitatory connections, respectively. The dynamics of the hidden (neuronal) states of each population can be described with the pairs of differential equations shown. There are four extrinsic connections: from SP to SS and DP (forward). Also, from DP to SP and II (backward). Intrinsic couplings are parametrized by $G_{1,..,10}$. Three regions comprise the network that is assumed to generate observed cross-spectral densities: V1 and left and right V5. These are shown on the top right. Forward connections were specified from V1 to V5 while backward connections were specified from V5 to V1. $\sigma(x_i)$ is a sigmoidal activation function which transforms post-synaptic potential into average spiking output. Finally, the external input to a brain source is denoted with u and enters SS.

described using the equations shown in **Figure 1**. Between source influences are mediated by extrinsic connections: Forward or backward (or both) connections, where forward connections originate from SP in one source and target SS and DP in another, while backward connections originate from DP and target SP and II. Exogenous (from other sources) inputs target SS.

Dynamic causal modelling for cross spectral data features

DCM is a Bayesian framework for inverting and comparing models of neural dynamics and the way these dynamics are translated into observations (in this case cross spectral data features). Therefore, it is useful to make a distinction between the neural model, which describes the hidden neural dynamics, and the observation model, which describes the mapping from neural states to observed responses. Usually, inference regarding the parameters of neural model is of interest (but see [34–38] for recent developments in multimodal fusion and applications of statistical decision theory in the context of DCM). A generative model is specified when the neural and forward model are combined and appropriately supplemented with prior constraints on the parameters. In this work, we used a specific DCM variant designed to deal with steady-state response called DCM for cross-spectral densities (CSD; [17,39]). Here, the generative model specifies how neural dynamics—driven by endogenous fluctuations—map to observed cross spectral densities. By linearizing the model around its fixed point, the resulting transfer functions specify how the endogenous fluctuations are mapped, through neural dynamics and the forward model, to the observed CSD. The power spectrum of the endogenous fluctuations

(innovations) is assumed to have a (parametrized) power law form: $g(\alpha, \beta, \omega) = \alpha\omega^{-\beta}$ with α and β the parameters controlling the amplitude and the slope (or more precisely the rate of decay) of spectral densities of the innovations noise. These parameters are estimated for each region separately.

In order to infer condition dependent changes in intrinsic coupling, the current DCM implementation of the CMC model described above, was supplemented with parameters encoding these changes as following [19]:

$$G_i = G_i^A + XG_i^B$$

Here, X encodes the conditions so that X = 0 for EO and X = 1 for EC condition. This implies that G_i^A encodes baseline intrinsic connectivity and here corresponds to the EO-state. Consequently, G_i^B encodes the modulation of the *i*-th intrinsic connection associated with the EC-state. Connectivity and other parameters of the neural model are shown in Table 1. The first 4 eigenmodes of the prior data covariance are used to project the channel data into a reduced sensor space (see [40] for more details). The cross spectral densities (CSD) that are used as data features are obtained from these 4 modes by fitting a Bayesian multivariate autoregressive model of order 12.

Table 1. Parameters of neural model (see **Error! Reference source not found.** for illustration of the neural model)

	Description	**Parametrisation**	**Prior**
τ_i	Postsynaptic time constant for subpopulation SS, SP, ii and DP	$(exp(\theta_k)*[2\ 2\ 16\ 28])$	$P(\theta_k) = N([0\ 0\ 0\ 0],1/32)$
$G^A_{1,..10}$	Baseline intrinsic connectivity	$exp(\theta^A_\gamma)$*[4, 4, 8, 4, 4, 2, 4, 4, 2, 1]*200	$P(\theta^A_G) = N(0,1/8)$
$G^B_{i=1,...10}$	Intrinsic connectivity modulation	$exp(\theta^B_\gamma)$	$P(\theta^B_G) = N(0,1/4)$
$A_{1,2,3,4}$	Extrinsic connectivity	$exp(\theta_A)*[1, ½, 1, ½]*200$	$P(\theta_A) = N(0,1/16)$
α,β	Amplitude and slope of the spectral innovations	$exp(\theta_{\alpha,\beta})$	$P(\theta_{\alpha,\beta}) = N(0,1/128)$

The forward model used here (the 'IMG'-option), treats each source as a patch on the cortical surface [41]. Each patch consists of a mixture of 6 spatial basis functions. The basis functions are taken from the eigenvectors of the lead field matrix of all dipoles whose origin was given by the MNI coordinates [0 -88 4] for V1 and [-44 -68 0] and [42 -72 0] for left and right V5,

respectively. DCMs with bad model fit (i.e. explained variance <50%) were removed from further analysis, in total 5 subjects were removed from the group-analysis.

Group level inference with parametric empirical Bayes

We used parametric empirical Bayes (PEB) to make inferences about extrinsic and intrinsic connectivity differences at the group level [21]. PEB uses a hierarchical model, which, at the first level, generates data from subject specific DCM parameters, and at the second level generates DCM parameters from group means, using a general linear model. The second level model characterizes between subject variability in terms of random effects. Here, we focused on group means of connectivity parameters. Using PEB, we obtained the posterior distribution of the (group mean) connectivity parameters and their condition-specific changes. In order to score the evidence for models with either extrinsic, V1 or V5 intrinsic connectivity modulations (or a combination thereof) we used Bayesian model reduction (BMR; [21]). We compared models with or without the following set of parameters: extrinsic modulations, V1 intrinsic modulations and V5 intrinsic modulations (in total, 8 models were considered). We also used a greedy search algorithm and Bayesian model reduction to prune second-level parameters from the PEB model with lowest evidence until we obtained 256 ‘best’ models. Bayesian model averaging (BMA) was subsequently applied to the reduced models to provide parameter estimates that accommodated for uncertainty over pruned or reduced models [42]. Inference on second level parameters—encoding group-mean intrinsic connectivity modulations—was based on the posterior probability (Pp) of a parameter being included in the model. The posterior means after BMA with Pp >.95 are treated as ‘significant’ in the sense that there is strong evidence for their contribution to the data.

Results

Power spectral results

Figure 2 displays the FDR-thresholded map of the frequency-by-channels t-values in image format. In addition, a 2-D topographical plot of the mean spectral power difference at 10.6Hz is shown and the mean power spectrum across subjects and 4 posterior electrodes (PO7, O1, O2 and PO6) are shown. The key things to note are significant differences around 10.6Hz. This difference was most pronounced over the posterior electrodes. However, a global effect can be observed in terms of statistical significance. Furthermore, positive and negative effects in higher frequency ranges were found. The positive effects were largely posteriorly localized (e.g., PO7, Oz, O2 and PO8; up to 23Hz), while the negative effects were localized to frontal electrodes (e.g., AF3, AF4, AF7, AF8; between 20 and 45Hz).

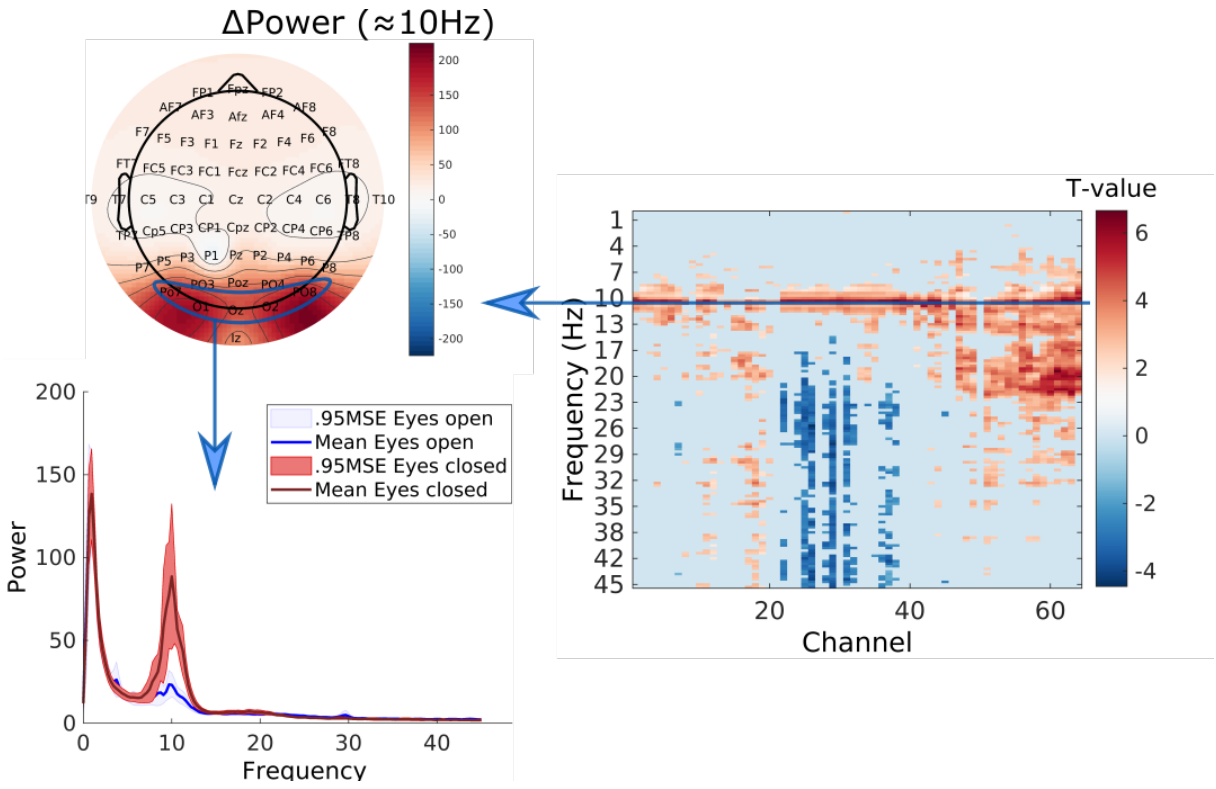

Figure 2. Results of the power spectral analysis. On the right, the FDR-thresholded t-values of all Channels x Frequencies are shown in image format. Given that we focus on alpha power differences, the topographic plot of the mean power difference (Δ Power) at 10.6 Hz is shown

on top-left. The mean power spectrum and 0.95 standard error intervals about the mean over channels PO7, Oz, O2 and PO8 for EO and EC are plotted at the bottom-left.

PEB model selection and parameter averaging

As a first step, we created 8 alternative PEB models to test which connectivity modulations are related to the difference between EO to EC conditions. We formed models by taking all combinations of the parameters that include all extrinsic modulations, V1 intrinsic modulations and V5 intrinsic connectivity modulations. In

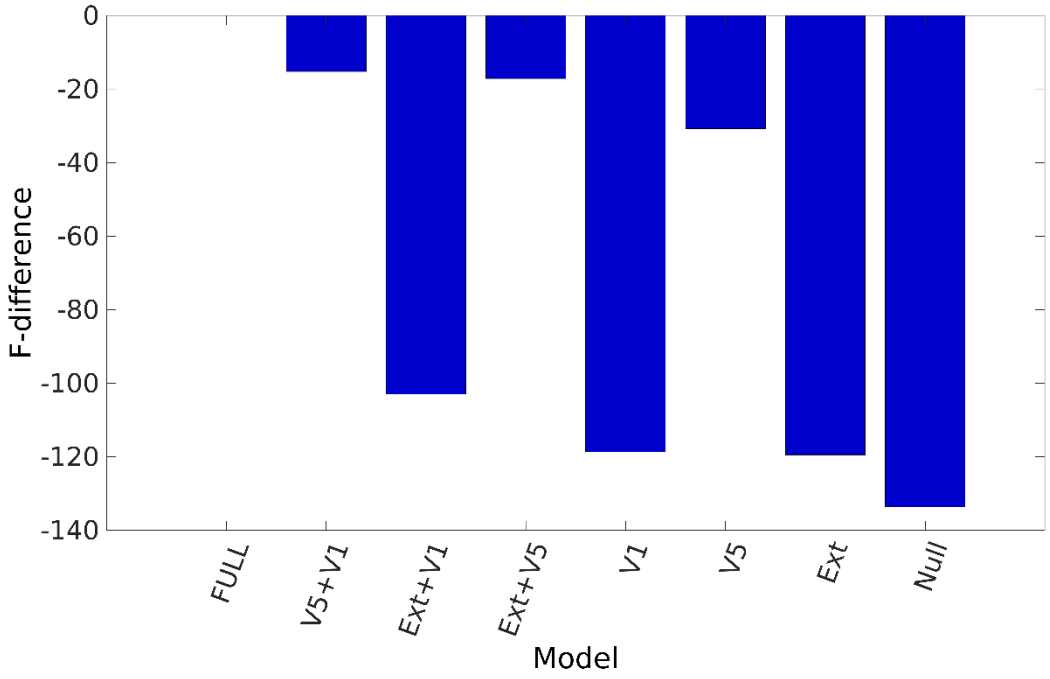

Figure 3, the log-evidence differences of the 8 models are shown. These differences are with respect to the full PEB model. We found that the full model had the largest evidence. The second-best model contained both V1 and V5 intrinsic modulations. The log-evidence difference between the best and second-best model was 15.23. This is larger than 3, which can be considered as very strong evidence in favour of the full model. In short, we found that both extrinsic and intrinsic modulations in V1 and V5 play an important role in explaining differences between EO and EC conditions. However, an interesting pattern can be observed. We see that models without V5 intrinsic modulations had much lower evidence relative to

models including V5 intrinsic modulations. This suggest that V5 intrinsic modulations were relatively important for explaining EO vs EC differences.

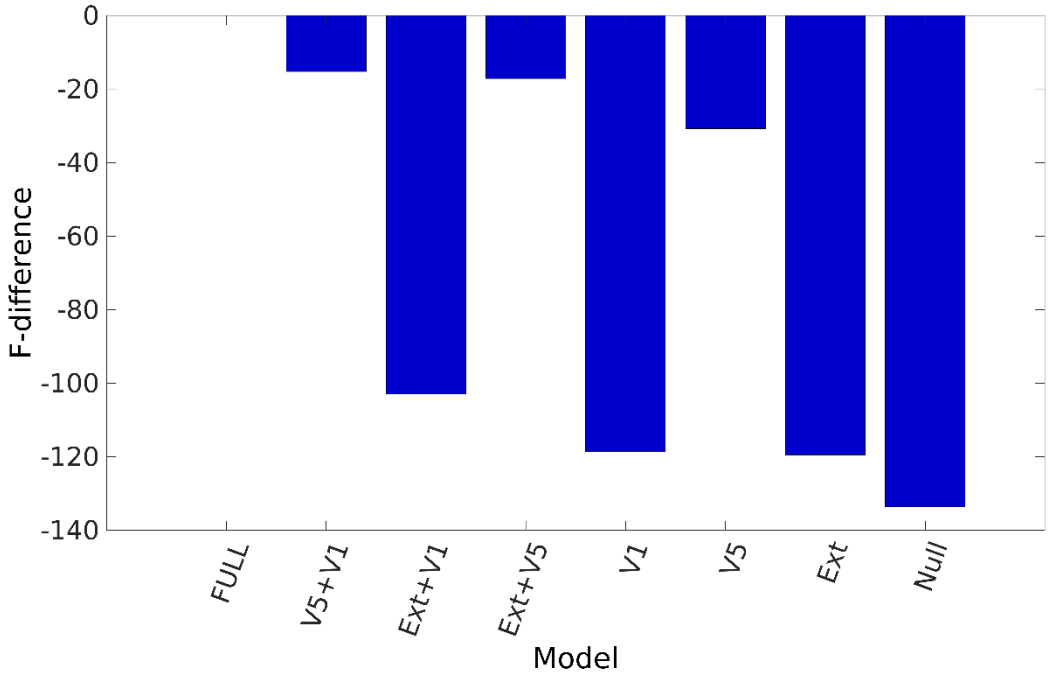

Figure 3. PEB model selection. The bar graph of the free energy (i.e., log evidence) differences from the full model are shown for the 8 PEB models considered. The models were formed by creating combinations of extrinsic modulations (Ext), V1 intrinsic modulations (V1) and V5 intrinsic modulations (V5). We observe that the full model has the highest (approximate) model evidence. In addition, models without V5 intrinsic modulation have smaller evidence compared to models that included V5 intrinsic modulation.

279 The Bayesian model average (BMA) estimates and 90% Bayesian confidence intervals of the

280 four extrinsic modulations can be found in Figure 4. We observe that all extrinsic connections.

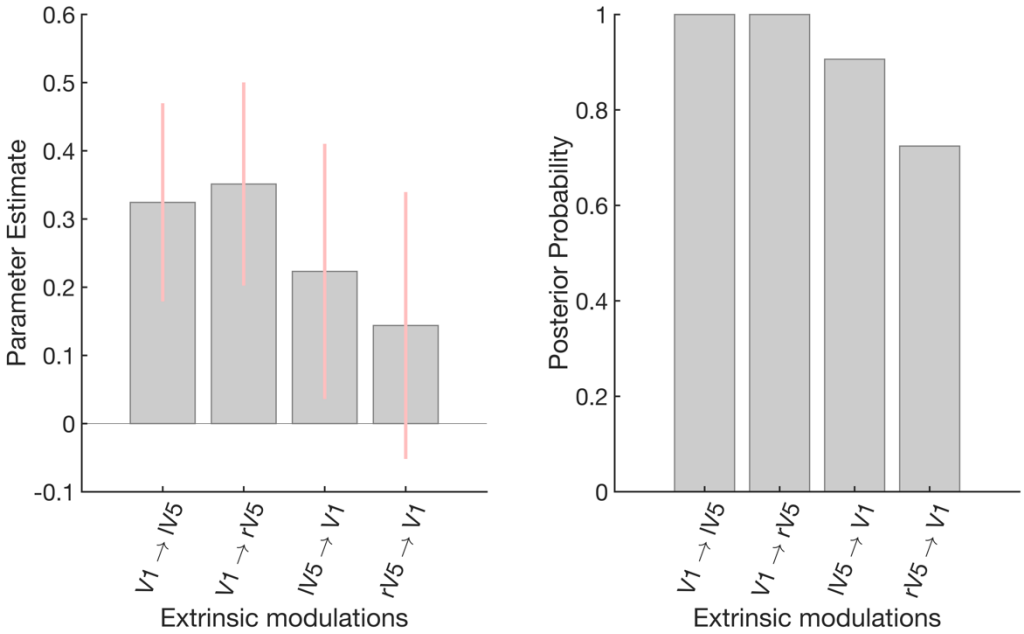

281 Figure 4. **Extrinsic connectivity modulations.** This figure shows the group-level results of
282 the extrinsic connectivity modulations associated with EC states (relative to EO). More
283 specifically, the mean posterior and 90% Bayesian confidence intervals (pink) after the greedy
284 search algorithm and Bayesian model averaging are shown. Note that the estimated
285 parameters are log-scale parameters (i.e., a positive log scale parameter means an increase).
286 The right panel shows the posterior probabilities of the extrinsic connection.

287 increase during EC. The posterior probabilities (Pp) are 100%, 100%, 90% and 72% for V1 →

288 lV5, V1 → rV5, lV5 → V1 and rV5 → V1, respectively

289

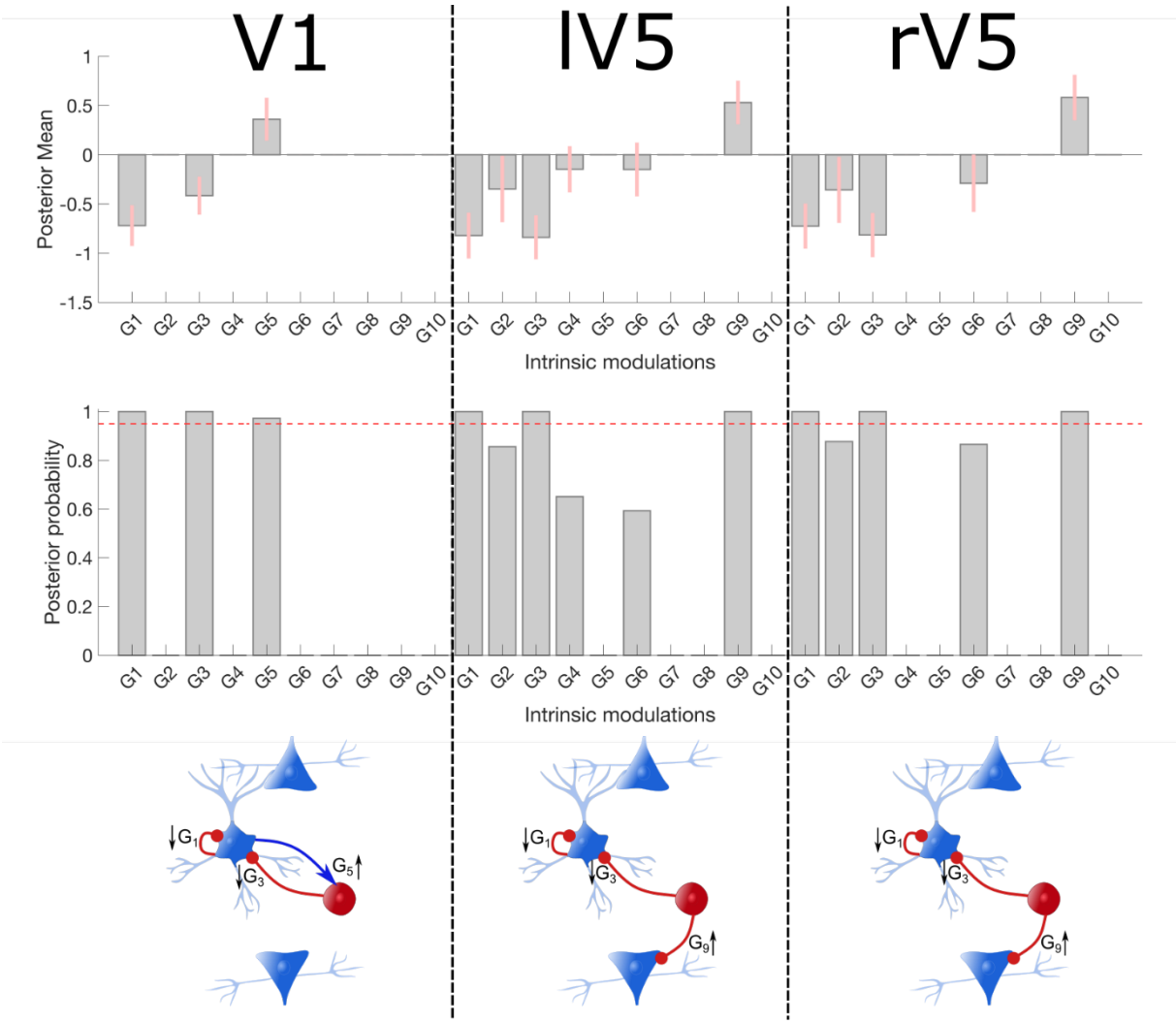

Figure 5. Intrinsic connectivity modulations. The figure reports the group-level results of the intrinsic connectivity modulations associated with EC states (relative to EO) in the three sources of interest. More specifically, the mean posterior and 90% Bayesian confidence interval (pink error bars) after the greedy search algorithm and Bayesian model averaging are shown in the top row. The middle row shows the corresponding posterior probabilities of the intrinsic modulations, the pink dotted lines correspond to a Pp of .95. Finally, the bottom is a schematic presentation of the modulation with Pp>.95 and the direction of the effect. Inhibitory connections are shown in red and excitatory in blue.

In order to characterise the contributions of the intrinsic and extrinsic connectivity modulations on the power spectrum, we performed a sensitivity analysis. Briefly, for each modulation

parameter, we examined the effect of a small parameter increment on the predicted power spectrum of the (reduced-) data of the posterior electrodes. More specifically, we added a small

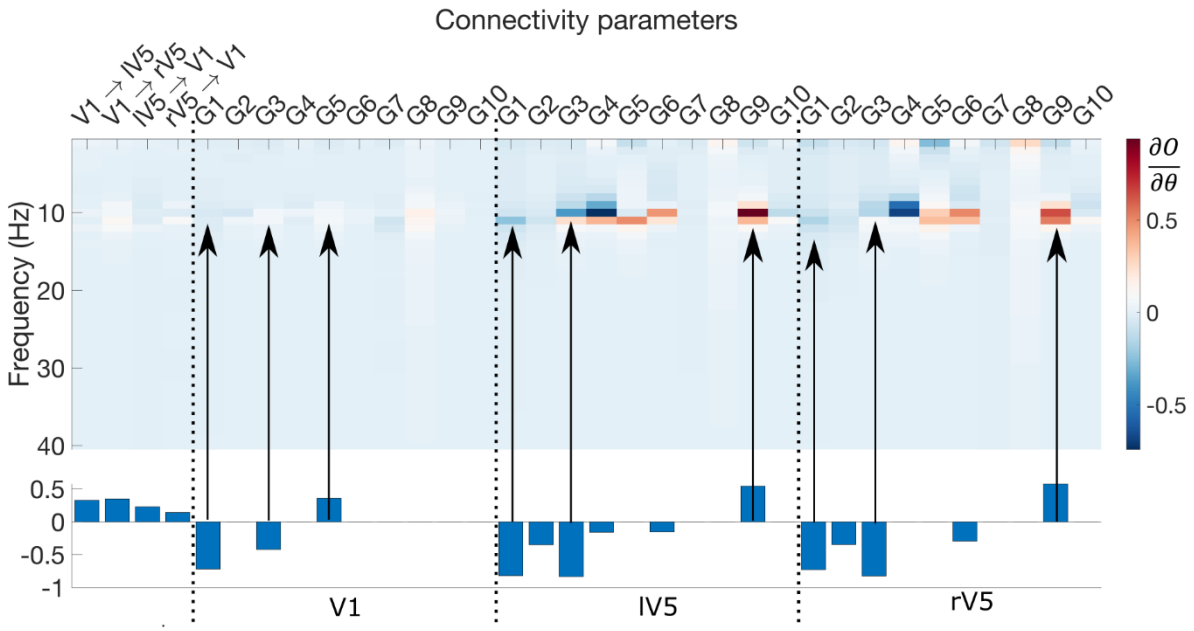

Figure 6. Sensitivity analysis. The results of the sensitivity analysis—averaged across subjects—are shown in image format. The group BMA results are provided in the lower part for comparison. Positive values (red) and negative values (blue) indicate that a parameter increase results in an increase and decrease, respectively of the predicted power spectrum. The arrows indicate the sensitivities for the significant intrinsic connectivity modulations that are shown in the lower part of the figure.

increment (e^{-6}) to the posterior mean of a certain parameter, while keeping the posterior means of the other parameters fixed. Technically, we are numerically evaluating the Jacobian of the generative model of the extrinsic and intrinsic connectivity modulations at their posterior means. This was repeated for every subject separately and subsequently averaged over subjects. The results are reported in **Figure 6** together with the posterior mean of the group-BMA

Positive (red) and negative (blue) values indicate that increasing or decreasing the parameter would result in increased and decreased power, respectively. Changes in intrinsic connectivity have a larger effect on the power spectrum compared to extrinsic connectivity and this is most pronounced for V5. In addition, we see clearly that the sensitivities are most pronounced within the alpha band (i.e., around 10Hz). If we consider the significant intrinsic modulation, we observe largest negative sensitivities for the inhibitory G_3 (II → SS) and G_1 (SS → SS)

modulations and positive sensitivities for the excitatory G_9(II → DP) modulations in left and right V5. The sensitivities of the significant modulations in V1 are much less pronounced compared to the sources in V5.

In summary, we found evidence that both extrinsic modulations between V1 and V5—as well as intrinsic modulations within V1 and V5—play an important role in the genesis of EO-EC power spectral differences. In addition, we found that the intrinsic modulations in bilateral V5, in particular the inhibitory connections, seem to play the greatest role. This speaks to the importance of local [dis]inhibition, within higher order visual cortex.

Discussion

In this work, we investigated the role of intrinsic and extrinsic connections within the occipital cortex in the generation of EO and EC alpha power differences. Using a publicly available data set, we first replicated previous findings that alpha-power is most pronounced during EC condition at posterior channels. Then, using DCM followed by PEB, our analysis showed that the model with the largest evidence contained both extrinsic and intrinsic connectivity modulations. Interestingly, our results showed that the intrinsic connections in V5 play a relatively larger role compared to the extrinsic connections and V1 intrinsic connections. Most inhibitory connections to SS-cells—the target population for endogenous neuronal fluctuations—decreased during EC. Overall, we found that decreased inhibitory connections within the higher order visual cortex seem to play an important role in underwriting EO-EC alpha power differences.

Several studies using biologically inspired models, fitted to EEG data, have been conducted in the context of EO-EC alpha power differences. In two recent studies by [43] and [43] the authors used a neural mass model of the same data set used in our study. In the first study, the authors investigated parameter identifiability of a 22-parameter neural mass model based on the EC data alone. They found that, using sampling-based inversion scheme a single parameter controlling inhibitory synaptic activity is directly identifiable. In a follow up paper, the

authors extended the model by incorporating modulatory parameters used for explaining EO-EC power differences. Their main finding was that a single modulatory parameter seems to explain best the alpha power difference; namely, a parameter controlling the tonic excitatory input to inhibitory populations. The authors argue in light of previous findings, that this external input is likely to be of thalamic origin. In relation to our modelling approach, several differences are important to consider. First, we used a neural mass model of multiple spatially defined and coupled occipital sources. This is to be contrasted with earlier studies, where no reference to coupled regions was made. Second, DCM combines a neural model of how different subpopulations within and between cortical sources interact, with a forward model of how post-synaptic potentials are mapped to observed data (here channel cross spectral densities). In comparison, the earlier studies mentioned above did not include an observation model. Thus, neural activity was not decoupled from volume conduction and observation noise (channel noise). Third, our approach used a variational Bayesian inversion scheme, which provides a lower bound on the log-model evidence, necessary for Bayesian model comparison. In other words, we identified the most plausible model, where both model fit and complexity were considered in scoring alternative models. Hartoyo et al. (2020) used particle swarm optimization and constrained half of the model parameters to be the same between the EO and EC conditions. They found that only 1 modulatory parameter provided the best explanation for generating EC-EO alpha differences. On the other hand, here we found that several modulatory parameters were identified for explaining spectral differences between EO and EC. Using BMC, we showed that both intrinsic and extrinsic connectivity parameters are necessary to explain the data. Fourth, Hartoyo et al. (2020) and Hartoyo et al. (2019), only used data from Cz to estimate the parameters of the model, while in the current work we used data from all EEG channels (projected to a reduced space).

In another related study, using empirical EO-EC EEG data for estimating the parameters of a neurophysiological model, the authors found multiple parameters that explained the difference between EO and EC [45]. Similarly, to the model by (Hartoyo et al., 2020) these authors used

data from a single electrode and did not include an observation model. They considered a thalamo-cortical model including intracortical and thalamocortical pathways and four type of neurons: cortical pyramidal (excitatory) and inhibitory neurons, thalamic reticular and thalamo-cortical relay neurons. They found that strong positive (excitatory) cortico-thalamic feedback and longer time constants underlie EC alpha power. One of the major strengths of this study is the incorporation of thalamocortical interactions, which is lacking in the current study. In principle, it is possible to incorporate the thalamus as a hidden source in DCM (i.e., the states of the hidden node do not contribute directly to the observed responses) to investigate bidirectional effect of thalamo-cortical dynamics (David, Maess, Eckstein, & Friederici, 2011). In essence, this approach would be the same as extending the current neural mass model to include additional subpopulations representing the thalamus. This approach was undertaken in the recent model by Min et al. (2020) by including excitatory and inhibitory neural populations in the thalamus. Their temporal dynamics are given by the well-known model of Lopes da Silva, Hoeks, Smits, & Zetterberg (1974) that describes thalamic oscillations [48,49]. The model includes thalamocortical relay (TC) and thalamic reticular nucleus (TRN) neurons. TC neurons project to the cortex, while TRN neurons surround the thalamus and regulate TC neuron activity by sending inhibitory signals. This model could be used in DCM to explain multimodal data (EEG and fMRI) from the thalamus and reveal differences in laminar dynamics (Friston et al., 2017; Pinotsis, 2020). Alternatively, it would be interesting to apply DCM to intracranial recordings where both thalamic and cortical areas are recorded simultaneously.

Given the role of inhibitory intrinsic connections found here, it is worth noting that cortical inhibition is largely mediated by GABAergic connections, while excitation is mediated by glutamatergic connections [50]. In a recent review paper by Lozano-Soldevilla (2018), the author discusses studies that used pharmacological modulation to study physiological mechanism underlying alpha rhythms. In their review, several findings are discussed in light of the so-called alpha power as inhibition principle [52]. Briefly, this principle states that alpha oscillations serve a functional inhibitory role which is implemented through physiological

401 inhibition (generated by GABAergic interneurons). Following this principle, one would expect
402 increased alpha in case of increased physiological inhibition. However, Lozano-Soldevilla
403 (2018) reviewed several lines of evidence showing pharmacologically enhanced inhibition
404 results in decreased rather than increased alpha. In addition, some studies have found that
405 sub-anaesthetic doses of ketamine (i.e. a glutamatergic excitatory NMDA receptor blocker)
406 resulted in decrease posterior alpha power in resting-state [53,54]. According to Wang (2010),
407 inhibition plays an important role in rhythmogenesis, either in an interneural network or via
408 excitatory-inhibitory loops. In sum, these studies are in line with our findings regarding the
409 importance of local inhibition in the generation of alpha rhythms during rest.

410 Functionally, two different brain configurations have been associated with EO and EC resting-
411 state condition: an exteroceptive state associated with attention, vigilance and ocular motor
412 activity and an interoceptive state associated with mental imagery and multisensory activity
413 [56–58]. Considering our results, one could suggest that inhibition in higher order visual areas
414 are the local manifestations of an interoceptive state that is triggered by eye closure.

415 Differences in power in a given band could be explained by changes in slope/aperiodic part
416 apart from modulations in pure oscillations [59]. In DCM, the shape of the observed spectra is
417 determined by the parametrized 1/f neural fluctuations (a.k.a., innovations) and importantly the
418 transfer functions that govern 'spectral bumps' in the output (Friston et al., 2012; Moran et al.,
419 2009). In this study, we assumed that during both EC and EO, the spectral shape of the
420 innovations remains the same and that differences are due to changes in connectivity. A
421 possible avenue for future research concerns the shape of the neural innovations driving V1
422 and V5. The current model could be augmented by allowing condition specific changes in either
423 the height, slope or both of the 1/f form of the neural innovations. In addition, condition specific
424 changes in the synaptic time-constants of the different neural populations could be examined.

425 Considering the aforementioned evidence, we suggest that dynamic causal modelling of
426 resting-state EO and EC conditions might provide a mechanistic insight into intrinsic

427 physiological mechanisms. This could be relevant for quantitative insights in clinical studies
428 but also studies that use pharmacologically altered states of consciousness.

429 Acknowledgements

430 This work has been funded by the Ghent University Research Council, grant number:
431 BOF17/GOA/004. KJF and DAP acknowledge financial support from UKRI ES/T01279X/1.
432 KJF is also supported by funding for the Wellcome Centre for Human Neuroimaging (Ref:
433 205103/Z/16/Z). FVDS receives funding by the Research Foundation – Flanders (FWO, project
434 No. 1267422N).

435 Data availability statement

436 We used a publicly available EEG data set in this work and can be found here:
437 https://physionet.org/content/eegmmidb/1.0.0/. The code used for model fitting and plotting
438 can be found on GitHub at: https://github.com/Frederikvdsteen/EO_OC_DCM.

439 References

440 1. Klimesch W. Alpha-band oscillations, attention, and controlled access to stored
441 information. Trends Cogn Sci. 2012;16: 606–617. doi:10.1016/j.tics.2012.10.007

442 2. Jensen O, Gelfand J, Kounios J, Lisman JE. Oscillations in the alpha band (9-12 Hz)
443 increase with memory load during retention in a short-term memory task. Cereb Cortex.
444 2002;12: 877–882. doi:10.1093/cercor/12.8.877

445 3. Pinotsis DA, Buschman TJ, Miller EK. Working Memory Load Modulates Neuronal
446 Coupling. Cereb Cortex. 2019;29: 1670–1681. doi:10.1093/cercor/bhy065

447 4. Worden MS, Foxe JJ, Wang N, Simpson G V. Anticipatory biasing of visuospatial
448 attention indexed by retinotopically specific alpha-band electroencephalography
449 increases over occipital cortex. J Neurosci. 2000;20: 1–6. doi:10.1523/jneurosci.20-06-

j0002.2000

5. Bastos AM, Donoghue JA, Brincat SL, Mahnke M, Yanar J, Correa J, et al. Neural effects of propofol-induced unconsciousness and its reversal using thalamic stimulation. Elife. 2021;10: 1–28. doi:10.7554/ELIFE.60824

6. Hughes SW, Lorincz ML, Blethyn K, Kékesi KA, Juhász G, Turmaine M, et al. Thalamic gap junctions control local neuronal synchrony and influence macroscopic oscillation amplitude during EEG alpha rhythms. Front Psychol. 2011;2: 1–11. doi:10.3389/fpsyg.2011.00193

7. Lőrincz ML, Kékesi KA, Juhász G, Crunelli V, Hughes SW. Temporal Framing of Thalamic Relay-Mode Firing by Phasic Inhibition during the Alpha Rhythm. Neuron. 2009;63: 683–696. doi:10.1016/J.NEURON.2009.08.012

8. Halgren M, Ulbert I, Bastuji H, Fabó D, Eross L, Rey M, et al. The generation and propagation of the human alpha rhythm. Proc Natl Acad Sci U S A. 2019;116: 23772–23782. doi:10.1073/pnas.1913092116

9. Lopes da Silva F. Neural mechanisms underlying brain waves: from neural membranes to networks. Electroencephalogr Clin Neurophysiol. 1991;79: 81–93.

10. Min BK, Kim HS, Pinotsis DA, Pantazis D. Thalamocortical inhibitory dynamics support conscious perception. Neuroimage. 2020;220: 117066. doi:10.1016/j.neuroimage.2020.117066

11. Cohen MX, Cavanagh JF, Slagter HA. Event-related potential activity in the basal ganglia differentiates rewards from nonrewards: Temporospatial principal components analysis and source localization of the feedback negativity: Commentary. Hum Brain Mapp. 2011;32: 2270–2271. doi:10.1002/hbm.21358

12. Seeber M, Cantonas LM, Hoevels M, Sesia T, Visser-Vandewalle V, Michel CM. Subcortical electrophysiological activity is detectable with high-density EEG source

475 imaging. Nat Commun. 2019;10: 1–7. doi:10.1038/s41467-019-08725-w

476 13. Michel CM, Murray MM, Lantz G, Gonzalez S, Spinelli L, Grave De Peralta R. EEG
477 source imaging. Clinical Neurophysiology. 2004. pp. 2195–2222.
478 doi:10.1016/j.clinph.2004.06.001

479 14. Van de Steen F, Faes L, Karahan E, Songsiri J, Valdes-Sosa PA, Marinazzo D. Critical
480 Comments on EEG Sensor Space Dynamical Connectivity Analysis. Brain Topogr.
481 2016; 1–12. doi:10.1007/s10548-016-0538-7

482 15. Attal Y, Schwartz D. Assessment of Subcortical Source Localization Using Deep Brain
483 Activity Imaging Model with Minimum Norm Operators: A MEG Study. PLoS One.
484 2013;8. doi:10.1371/journal.pone.0059856

485 16. Michel CM, Brunet D. EEG source imaging: A practical review of the analysis steps.
486 Front Neurol. 2019;10. doi:10.3389/fneur.2019.00325

487 17. Friston KJ, Bastos A, Litvak V, Stephan KE, Fries P, Moran RJ. DCM for complex-valued
488 data: Cross-spectra, coherence and phase-delays. Neuroimage. 2012;59: 439–455.
489 doi:10.1016/j.neuroimage.2011.07.048

490 18. David O, Guillemain I, Saillet S, Reyt S, Deransart C, Segebarth C, et al. Identifying
491 neural drivers with functional MRI: an electrophysiological validation. PLoS Biol. 2008;6.
492 doi:10.1371/journal.pbio.0060315

493 19. Pinotsis DA, Brunet N, Bastos A, Bosman CA, Litvak V, Fries P, et al. Contrast gain
494 control and horizontal interactions in V1: A DCM study. Neuroimage. 2014;92: 143–155.
495 doi:10.1016/J.NEUROIMAGE.2014.01.047

496 20. Pinotsis DA, Friston KJ. Extracting novel information from neuroimaging data using
497 neural fields. EPJ Nonlinear Biomed Phys. 2014;2: 5. doi:10.1140/epjnbp18

498 21. Friston K, Litvak V, Oswal A, Razi A, Stephan KE, Van Wijk BCM, et al. Bayesian model

reduction and empirical Bayes for group (DCM) studies. Neuroimage. 2016;128: 413–431. doi:10.1016/j.neuroimage.2015.11.015

22. Pinotsis DA, Perry G, Litvak V, Singh KD, Friston KJ. Intersubject variability and induced gamma in the visual cortex: DCM with empirical Bayes and neural fields. Hum Brain Mapp. 2016;37: 4597–4614. doi:10.1002/hbm.23331

23. Wan L, Huang H, Schwab N, Tanner J, Rajan A, Lam NB, et al. From eyes-closed to eyes-open: Role of cholinergic projections in EC-to-EO alpha reactivity revealed by combining EEG and MRI. Hum Brain Mapp. 2018; 1–12. doi:10.1002/hbm.24395

24. Hanslmayr S, Sauseng P, Doppelmayr M, Schabus M, Klimesch W. Increasing individual upper alpha power by neurofeedback improves cognitive performance in human subjects. Appl Psychophysiol Biofeedback. 2005;30: 1–10. doi:10.1007/s10484-005-2169-8

25. Babiloni C, Lizio R, Vecchio F, Frisoni GB, Pievani M, Geroldi C, et al. Reactivity of cortical alpha rhythms to eye opening in mild cognitive impairment and Alzheimer's disease: An EEG study. J Alzheimer's Dis. 2010;22: 1047–1064. doi:10.3233/JAD-2010-100798

26. Schalk G, McFarland DJ, Hinterberger T, Birbaumer N, Wolpaw JR. BCI2000: A General-Purpose Brain-Computer Interface (BCI) System. IEEE Trans Biomed Eng. 2004;51: 1034–1043. doi:10.1109/TBME.2004.827072

27. Goldberger AL, Amaral LA, Glass L, Hausdorff JM, Ivanov PC, Mark RG, et al. PhysioBank, PhysioToolkit, and PhysioNet: components of a new research resource for complex physiologic signals. Circulation. 2000;101: E215-20. doi:10.1161/01.CIR.101.23.E215

28. Chatrian GE, Lettich E, Nelson PL. Ten Percent Electrode System for Topographic Studies of Spontaneous and Evoked EEG Activities. Am J EEG Technol. 1985;25: 83–

524 92. doi:10.1080/00029238.1985.11080163

525 29. Delorme A, Makeig S. EEGLAB: an open source toolbox for analysis of single-trial EEG
526 dynamics including independent component analysis. J Neurosci Methods. 2004;134:
527 9–21. doi:10.1016/J.JNEUMETH.2003.10.009

528 30. Van de Steen F, Almgren HBJ, Razi A, Friston KJ, Marinazzo D. Dynamic causal
529 modelling of fluctuating connectivity in resting-state EEG. bioRxiv. 2018;189: 476–484.
530 doi:10.1101/303933

531 31. Benjamini Y, Hochberg Y. Controlling the False Discovery Rate: A Practical and
532 Powerful Approach to Multiple Testing. J R Stat Soc Ser B. 1995. doi:10.1111/j.2517-
533 6161.1995.tb02031.x

534 32. Pinotsis DA, Schwarzkopf DS, Litvak V, Rees G, Barnes G, Friston KJ. Dynamic causal
535 modelling of lateral interactions in the visual cortex. Neuroimage. 2013;66: 563–576.
536 doi:10.1016/j.neuroimage.2012.10.078

537 33. Bastos AM, Usrey WM, Adams RA, Mangun GR, Fries P, Friston KJ. Canonical
538 Microcircuits for Predictive Coding. Neuron. Cell Press; 2012. pp. 695–711.
539 doi:10.1016/j.neuron.2012.10.038

540 34. Pinotsis DA. Statistical decision theory and multiscale analyses of human brain data. J
541 Neurosci Methods. 2020;346: 108912. doi:10.1016/j.jneumeth.2020.108912

542 35. Friston KJ, Preller KH, Mathys C, Cagnan H, Heinzle J, Razi A, et al. Dynamic causal
543 modelling revisited. Neuroimage. 2017; 0–1. doi:10.1016/j.neuroimage.2017.02.045

544 36. Jafarian A, Litvak V, Cagnan H, Friston KJ, Zeidman P. Comparing dynamic causal
545 models of neurovascular coupling with fMRI and EEG/MEG. Neuroimage. 2020;
546 116734. doi:10.1016/j.neuroimage.2020.116734

547 37. Pinotsis DA, Geerts JP, Pinto L, FitzGerald THB, Litvak V, Auksztulewicz R, et al.

548 Linking canonical microcircuits and neuronal activity: Dynamic causal modelling of
549 laminar recordings. Neuroimage. 2017;146: 355–366.
550 doi:10.1016/j.neuroimage.2016.11.041

551 38. Higgins C, Liu Y, Vidaurre D, Kurth-Nelson Z, Dolan R, Behrens T, et al. Replay bursts
552 in humans coincide with activation of the default mode and parietal alpha networks.
553 Neuron. 2021;109: 882-893.e7. doi:10.1016/j.neuron.2020.12.007

554 39. Moran RJ, Stephan KE, Seidenbecher T, Pape HC, Dolan RJ, Friston KJ. Dynamic
555 causal models of steady-state responses. Neuroimage. 2009;44: 796–811.
556 doi:10.1016/j.neuroimage.2008.09.048

557 40. Fastenrath M, Friston KJ, Kiebel SJ. NeuroImage Dynamical causal modelling for M /
558 EEG : Spatial and temporal symmetry constraints. Neuroimage. 2009;44: 154–163.
559 doi:10.1016/j.neuroimage.2008.07.041

560 41. Daunizeau J, Kiebel SJ, Friston KJ. Dynamic causal modelling of distributed
561 electromagnetic responses. Neuroimage. 2009;47: 590–601.
562 doi:10.1016/j.neuroimage.2009.04.062

563 42. Friston K, Penny W. Post hoc Bayesian model selection. Neuroimage. 2011;56: 2089–
564 2099. doi:10.1016/J.NEUROIMAGE.2011.03.062

565 43. Hartoyo A, Cadusch PJ, Liley DTJ, Hicks DG. Inferring a simple mechanism for alpha-
566 blocking by fitting a neural population model to EEG spectra. PLoS Comput Biol.
567 2020;16: 1–19. doi:10.1371/journal.pcbi.1007662

568 44. Hartoyo A, Cadusch PJ, Liley DTJ, Hicks DG. Parameter estimation and identifiability in
569 a neural population model for electro-cortical activity. PLoS Comput Biol. 2019;15: 1–
570 27. doi:10.1371/journal.pcbi.1006694

571 45. Rowe DL, Robinson PA, Rennie CJ. Estimation of neurophysiological parameters from
572 the waking EEG using a biophysical model of brain dynamics. J Theor Biol. 2004;231:

413–433. doi:10.1016/j.jtbi.2004.07.004

46. David O, Maess B, Eckstein K, Friederici AD. Dynamic Causal Modeling of Subcortical Connectivity of Language. J Neurosci. 2011;31: 2712–2717. doi:10.1523/JNEUROSCI.3433-10.2011

47. Lopes da Silva FH, Hoeks A, Smits H, Zetterberg LH. Model of brain rhythmic activity. Kybernetik. 1974;15: 27–37. doi:10.1007/BF00270757

48. Costa MS, Weigenand A, Ngo H V. A Thalamocortical Neural Mass Model of the EEG during NREM Sleep and Its Response to Auditory Stimulation. 2016; 1–20. doi:10.1371/journal.pcbi.1005022

49. Haghighi HS, Markazi AHD. OPEN A new description of epileptic seizures based on dynamic analysis of a thalamocortical model. Sci Rep. 2017; 1–10. doi:10.1038/s41598-017-13126-4

50. Legon W, Punzell S, Dowlati E, Adams SE, Stiles AB, Moran RJ. Altered Prefrontal Excitation/Inhibition Balance and Prefrontal Output: Markers of Aging in Human Memory Networks. Cereb Cortex. 2016;26: 4315–4326. doi:10.1093/cercor/bhv200

51. Lozano-Soldevilla D. On the physiological modulation and potential mechanisms underlying parieto-occipital alpha oscillations. Front Comput Neurosci. 2018;12: 1–19. doi:10.3389/fncom.2018.00023

52. Klimesch W, Sauseng P, Hanslmayr S. EEG alpha oscillations: The inhibition-timing hypothesis. Brain Res Rev. 2007;53: 63–88. doi:10.1016/j.brainresrev.2006.06.003

53. de la Salle S, Choueiry J, Shah D, Bowers H, McIntosh J, Ilivitsky V, et al. Effects of ketamine on resting-state EEG activity and their relationship to perceptual/dissociative symptoms in healthy humans. Front Pharmacol. 2016;7: 1–14. doi:10.3389/fphar.2016.00348

597 54. Rivolta D, Heidegger T, Scheller B, Sauer A, Schaum M, Birkner K, et al. Ketamine
598 dysregulates the amplitude and connectivity of high-frequency oscillations in cortical-
599 subcortical networks in humans: Evidence from resting-state
600 magnetoencephalography-recordings. Schizophr Bull. 2015;41: 1105–1114.
601 doi:10.1093/schbul/sbv051

602 55. Wang X. Neurophysiological and Computational Principles of Cortical Rhythms in
603 Cognition. Physiol Rev. 2010;90: 1195–1268.
604 doi:10.1152/physrev.00035.2008.Neurophysiological

605 56. Marx E, Deutschländer A, Stephan T, Dieterich M, Wiesmann M, Brandt T. Eyes open
606 and eyes closed as rest conditions: Impact on brain activation patterns. Neuroimage.
607 2004;21: 1818–1824. doi:10.1016/j.neuroimage.2003.12.026

608 57. Marx E, Stephan T, Nolte A, Deutschländer A, Seelos KC, Dieterich M, et al. Eye closure
609 in darkness animates sensory systems. Neuroimage. 2003;19: 924–934.
610 doi:10.1016/S1053-8119(03)00150-2

611 58. Costumero V, Bueichekú E, Adrián-Ventura J, Ávila C. Opening or closing eyes at rest
612 modulates the functional connectivity of V1 with default and salience networks. Sci Rep.
613 2020;10: 1–10. doi:10.1038/s41598-020-66100-y

614 59. Donoghue T, Haller M, Peterson EJ, Varma P, Sebastian P, Gao R, et al.
615 Parameterizing neural power spectra into periodic and aperiodic components. Nat
616 Neurosci. 2020;23: 1655–1665. doi:10.1038/s41593-020-00744-x

617